

**Demonstration of a Wire Suspension for  
Virtual Flight Testing in a Wind Tunnel**

John C. Magill, Paolo Cataldi, Joseph R. Morency, and Daniel X. Hammer  
Physical Sciences Inc., Andover, MA 01810

Riley Burgess and Edward Jeter  
Naval Air Warfare Center/Weapons Division, China Lake, CA

Accepted for Publication (2/4/09)  
AIAA Journal of Spacecraft and Rockets

Tracking No. 39188  
Log No. A30281

Subject Index:  
32300 Missile Dynamics; 32400 Missile Guidance and Control;  
40900 Research Facilities and Instrumentation

Upload to: [www.writetrack.org](http://www.writetrack.org)  
Uploaded Source Files, Copyright, Subject Index (2/27/09)

(Contract No. PSI-1369)

February 2009

# Report Documentation Page

Form Approved  
OMB No. 0704-0188

Public reporting burden for the collection of information is estimated to average 1 hour per response, including the time for reviewing instructions, searching existing data sources, gathering and maintaining the data needed, and completing and reviewing the collection of information. Send comments regarding this burden estimate or any other aspect of this collection of information, including suggestions for reducing this burden, to Washington Headquarters Services, Directorate for Information Operations and Reports, 1215 Jefferson Davis Highway, Suite 1204, Arlington VA 22202-4302. Respondents should be aware that notwithstanding any other provision of law, no person shall be subject to a penalty for failing to comply with a collection of information if it does not display a currently valid OMB control number.

1. REPORT DATE <b>FEB 2009</b>		2. REPORT TYPE		3. DATES COVERED <b>00-00-2009 to 00-00-2009</b>	
4. TITLE AND SUBTITLE <b>Demonstration of a Wire Suspension for Virtual Flight Testing in a Wind Tunnel</b>				5a. CONTRACT NUMBER	
				5b. GRANT NUMBER	
				5c. PROGRAM ELEMENT NUMBER	
6. AUTHOR(S)				5d. PROJECT NUMBER	
				5e. TASK NUMBER	
				5f. WORK UNIT NUMBER	
7. PERFORMING ORGANIZATION NAME(S) AND ADDRESS(ES) <b>Physical Sciences Inc,20 New England Business Center,Andover,MA,01810-1077</b>				8. PERFORMING ORGANIZATION REPORT NUMBER	
9. SPONSORING/MONITORING AGENCY NAME(S) AND ADDRESS(ES)				10. SPONSOR/MONITOR'S ACRONYM(S)	
				11. SPONSOR/MONITOR'S REPORT NUMBER(S)	
12. DISTRIBUTION/AVAILABILITY STATEMENT <b>Approved for public release; distribution unlimited</b>					
13. SUPPLEMENTARY NOTES					
14. ABSTRACT					
15. SUBJECT TERMS					
16. SECURITY CLASSIFICATION OF:			17. LIMITATION OF ABSTRACT	18. NUMBER OF PAGES	19a. NAME OF RESPONSIBLE PERSON
a. REPORT <b>unclassified</b>	b. ABSTRACT <b>unclassified</b>	c. THIS PAGE <b>unclassified</b>			

# Demonstration of a Wire Suspension for Virtual Flight Testing in a Wind Tunnel

John C. Magill,<sup>\*</sup> Paolo Cataldi,<sup>†</sup> Joseph R. Morency,<sup>‡</sup> and Daniel X. Hammer<sup>§</sup>  
*Physical Sciences Inc., Andover, MA 01810*

Riley Burgess<sup>\*\*</sup> and Edward Jeter<sup>††</sup>  
*Naval Air Warfare Center/Weapons Division, China Lake, CA*

**This paper describes the development of a wire suspension system for dynamic testing of missiles in a wind tunnel. The system restrains the missile, permits motion in three rotational degrees of freedom, and measures forces on the model. The apparatus allows testing of missile control systems in the wind tunnel, reducing the cost and risk of a flight test program. Hydraulic actuators control cable tension and model position. Bearings provide free roll and pitch, while yaw motion is created by the cable actuation system and a repetitive learning controller. The paper describes the cable arrangement, force balance, bearings, closed-loop hydraulic control, and the repetitive-learning controller. Two sets of tests were conducted with the BOA missile (a sidewinder variant) in the HIVAS facility at the China Lake Naval Weapons Center. The tests, conducted at M=0.4-0.6, demonstrate functionality of the system in a series of missile pitch and yaw maneuvers. The learning controller is shown to learn an s-maneuver in the yaw plane.**

## Nomenclature

$C_{M_\alpha}, C_{M_q}$	=	model stability parameters
$i_{v,j}$	=	current to $j^{\text{th}}$ servo valve
$I_{yy}$	=	moment of inertia of missile about the pitch axis
$I_{zz}$	=	moment of inertia of missile about the yaw axis
$K_m$	=	moment gain in learning algorithm
$K_p$	=	cylinder position loop proportional gain
$K_d$	=	cylinder position loop derivative gain
$\ell_i$	=	position of cable $i$
$\bar{\ell}_i$	=	starting length for cable $i$
$N_{i,n}$	=	yawing moment for learning iteration $i$ at time step $n$
$q_{j,d}$	=	cylinder $j$ desired position
$q_j$	=	cylinder $j$ measured position
$\Delta T$	=	control time step
$\bar{W}_{i,n}$	=	yawing moment high-pass filter output in learning algorithm for learning iteration $i$ at time step $n$

---

<sup>\*</sup> Principal Research Scientist, Physical Sciences Inc., 20 New England Business Center, Andover, MA 01810-1077, AIAA Senior Member.

<sup>†</sup> Senior Project Specialist, Physical Sciences Inc., 20 New England Business Center, Andover, MA 01810-1077, AIAA Member.

<sup>‡</sup> Manufacturing Engineering Manager, Physical Sciences Inc., 20 New England Business Center, Andover, MA 01810-1077, Non-Member.

<sup>§</sup> Group Leader, Biomedical Imaging, Physical Sciences Inc., 20 New England Business Center, Andover, MA 01810-1077, Non-Member Grade.

<sup>\*\*</sup> Missile Integration Specialist, Naval Air Warfare Center/Weapons Division, China Lake, CA 93555.

<sup>††</sup> Technical Staff, Naval Air Warfare Center/Weapons Division, China Lake, CA, Senior AIAA Member.

- $W_{i,n}$  =  $\overline{W}_{i,n}$  normalized by its maximum value
- $\dot{x}, \dot{y}, \dot{z}$  = model translation rates
- $\overline{\Psi}_{i,n}$  = change to yaw motion profile applied to iteration i, time step n
- $\Psi_{i,n}$  = yaw motion profile for iteration i at time step n
- $\theta$  = pitch angle
- $\tau_w, \tau_v$  = time constant for filters in learning algorithm

## Introduction

In an effort to match test technology to the pace of advancement in maneuverability of missiles, engineers at the USAF Arnold Engineering Development Center (AEDC) began many years ago to develop new dynamic wind tunnel test techniques.<sup>1</sup> These techniques, now known as Virtual Flight Tests (VFTs), are intended to evaluate guidance and control systems, aeroelastic phenomena, and flows around maneuvering bodies. The purpose of VFT is to provide advanced dynamic test capabilities to developers of missiles and other flight vehicles.

In a VFT, the test article will be supported in the wind tunnel such that it can pivot freely while being restrained from translational motion. The vehicle attitude control system can be tested over a range of flight angles, so that unexpected dynamic behaviors can be identified and control systems can be tested and refined. By permitting pre-flight control evaluation, VFT can reduce the risk, and hence the potential cost, associated with flight testing.

In its most basic embodiment, a VFT apparatus must support the test article in the wind tunnel while allowing it to rotate about one or more axes (roll, pitch, and yaw). The rotational damping due to the mount must be small relative to the aerodynamic loads on the vehicle, so that the mount does not render the missile much more stable than the in-flight behavior. In fact, a key use of the device will be to determine whether a vehicle control system is able to maintain stable flight over a range of conditions. Large parasitic damping from the mount would produce false results.

To increase the amount of data available from a test, we have engineered a system that meets the minimum needs and adds a number of sensing capabilities. These include angle measurements and multi-component aerodynamic load measurements. Because past experience showed that aeroelastic instabilities in the mount structure can be excited during maneuver tests, the new system also includes an active hydraulic damping system.

AEDC and China Lake engineers previously demonstrated an 8-wire system in the HIVAS facility at China Lake.<sup>2</sup> These tests were performed in the same facility with the same missile as the tests described in this report. PSI later demonstrated a small-scale six-wire system in a 40 in. wind tunnel at Georgia Tech.<sup>3</sup> Drawing on the experience of the previous tests, the latest generation of the wire suspension systems was built and tested. Physical

Sciences Inc., the Naval Air Warfare Center/China Lake, and AEDC recently completed the most sophisticated Virtual Flight Tests to date. This paper summarizes the system design, and then describes several virtual flight tests performed with the BOA-1SC PTV-2 air-to-air missile

Figure 1 shows the configuration for the system as it would be applied to a wind tunnel test section. The system consisted of six cables supporting the model. The model was attached to a collar assembly at the center of the test section. Each cable was attached to a hydraulic cylinder to provide cable pre-tension, damp elastic oscillations of the cable/model structure, and pull or relax the cable to produce yaw motion.

The collar assembly included pairs of roll and pitch bearings to provide free motion in those axes. The collar also included a strain gage balance that is able to measure axial, normal, and side forces, as well as yawing moment. The hydraulic actuators imparted yaw to the model by pulling and relaxing the cables. This provided an apparent yaw degree of freedom. A learning controller used yawing moment measurements from the balance, acquired during several repetitions of a maneuver, to determine the yaw motion resulting from a particular set of control inputs. This apparent yaw approach was chosen over the previous approach of incorporating yaw bearings<sup>3</sup> because the structure supporting additional bearings produced substantial aerodynamic interference with the model.

The specific design requirements are summarized here:

- Maximum normal force of 4000 lb static + 5000 lb dynamic
- Maximum axial force of 500 lb static + 400 lb dynamic
- Maximum induced motion due to elastic response not to exceed 1 in. and 2 g's
- Rotational friction torque not more than 10 in.-lb
- 360 deg roll
- $\pm 30$  deg yaw
- $\pm 180$  deg pitch
- Minimum safety factor of 3.0 based on yield strength.

### **Sensor and Actuator Suite**

The VFT system included sensors to measure desired test data, perform control functions, and maintain safe test conditions. The full sensor suite included:

1. Four-component strain gage balance to sense normal force, axial force, side force, and yawing moment
2. Load cells to sense cable tension

3. Hydraulic actuator position sensors
4. Quadrature encoders to sense roll and pitch angles
5. Collar accelerometer to sense model motion.

The VFT collar was designed to accommodate roll and pitch slip rings to carry signals and power across the bearings, but they were not needed for these tests. The balance and accelerometer cables were directly connected since pitch was limited, and the model was internally powered.

### **System Mechanical Design Overview**

Figure 2 shows the collar assembly that enabled the model to pitch and roll, while measuring axial, normal, and side forces, as well as yawing moment. The test model's fore and aft sections were attached to the model hubs on either end of the collar. They were connected by the roll shaft, which rotates in a pair of bearings. These bearings supported both radial and axial loads. Loads were transmitted to the bearing housing, so that the roll shaft was loaded only by pre-load tension and roll torsion. Missile bending moments were transmitted between fore and aft model sections through the balance body. An optical encoder at one end of the bearing housing measures roll angle with a resolution of 0.09 deg.

This collar design provides bearings at a diameter much smaller than the test article, resulting in two key advantages. First, smaller bearings produce less rolling friction. Second, the bearings do not need to match the missile OD. To change to a model of any diameter larger than the size of the housing, it is necessary only to fabricate a shroud for the bearings that matches the size of the missile (see Fig. 3).

A key component of the bearing selection criteria was the bearing friction torque. Using manufacturer's data, we estimated the break-away and dynamic friction under load for each of the combinations above. Procedures for estimating bearing friction can be found in text books and in manufacturer's literature.<sup>4,5</sup> Deep-groove ball bearings were chosen for the roll axis. The pitch bearings present a greater challenge in friction, since they must carry the substantial axial load due to cable pre-tension. Analysis showed that the best choice of pitch bearings is a combination of a ball thrust bearing, which will carry an axial load, and a radial ball bearing to support the radial loads.

To determine whether the anticipated bearing friction is acceptable, we modeled the impact of the static and dynamic friction on a candidate missile model. The model was created using MATLAB/ SIMULINK. The model is a simple rotational spring-mass-damper. This represents the pitch dynamics of a missile model constrained in a wind tunnel.

The missile used in the simulation had the following properties, estimated by examining published data for a variety of missiles:

- Pitch stiffness ( $C_{M_\alpha}$ ): -20
- Pitch damping ( $C_{M_q}$ ): -500
- Diameter: 6 in.
- Length: 60 in.
- Moment of inertia ( $I_{yy}$ ): 13 slg-ft<sup>2</sup>
- Freestream velocity: 900 ft/s.
- Pitch Bearing Friction:
  - Case I: No friction
  - Case II: 12 in.-lb. rolling torque, 24 in.-lb. starting torque
  - Case III: 30 in.-lb. rolling torque, 60 in.-lb. starting torque

Simulations were carried out for three bearing friction levels (Fig. 4) to predict the response of a model disturbed 10 deg from its trim angle of attack. For case II, which is approximately the bearing friction level estimated for our design, the time history of the pitch angle is nearly indistinguishable from the frictionless except at very low pitch excursions. This indicates that the bearing friction will not seriously impede the evaluation of damping parameters. Even in case III, which has nearly twice the friction estimated for our design, the impact on pitch oscillation is modest.

In general, attachment of a missile to the collar will change the structural properties of the airframe – most notable the bending and torsional stiffness. For the demonstration tests described here, this was not specifically addressed. When aeroelastic characteristics must be accurately recreated in the test, special attention to the roll shaft stiffness and the hub/attachment details will be required. We anticipate that this would include both computer modeling of the elastic properties and tests of the stiffness and natural frequencies of the structure after assembly of the test configuration.

Pitch action was provided by bearings mounted in the cable vertex block. An optical encoder attached to one of these blocks sensed pitch position with a resolution of 0.09 deg. The pitch axle carried approximately 5000 lb of cable pre-tension load. To avoid overloading the bearing housing and potentially distorting the bearings, a tension

box was incorporated in the collar design. This element attached on opposite sides to the pitch axle and provided a mounting point for the balance.

The strain gauge balance<sup>7-11</sup> was formed by a pair of flexure plates that flank the roll housing. They were instrumented with a total of four full bridges. Fore and aft side force bridges sensed both net side force and yawing moment. A third bridge measured the normal force, and the fourth was applied to the main axial force flexure.

To minimize aerodynamic interference, the collar was designed to be as small as possible while supporting the loads at required safety factors. The degree of interference with the flow over the airframe will depend on body diameter, fin geometry, control actuators, and distance of fins and control surfaces from the collar. We did not quantify the effects of the collar on flow over the test vehicle airframe in initial tests, but we recognize this as an important issue that should be addressed in future tests.

The entire balance was made from Grade 300 Maraging Steel (ASTM A538) with a yield and ultimate tensile strength of 315,000 and 321,000 psi, respectively. The plates were electron beam (EB) welded to the roll housing.

The cables were formed from two sections. A 1/2 in. rigid round steel (17-4 PH stainless) rod attached to the collar and extends past the outer boundary of the test section. Outside of the tunnel, a 1/2 in. flexible steel cable was attached to the solid rod. The cable was a 6 x 19 Extra-Improved Plow Steel wire-core wire rope. The flexible cables were routed over a pulley to provide flexibility in mounting the hydraulic cylinder modules. Forces in the cables were measured using 1210-series load cells from Interface Inc. The load cells chosen had a rated load range of up to 10,000 lb.

Each cable was pulled into tension by a 2.5 in. diameter hydraulic cylinder with a 3 in. stroke. Flow in and out of the cylinder was controlled by a two-stage servo valve from Moog Inc.<sup>TM</sup> Pressure for the system was provided from a 25 HP hydraulic pump. The pump was water-cooled and could provide 10 GPM hydraulic fluid at 3000 psig.

The hydraulic cylinders located at the end of each cable served three purposes. They provided cable pre-tension control, they imparted yawing motion, and they could be used as part of a control system to damp unsteady oscillations in the structure.

Figure 5 shows how the hydraulic system operated. A hydraulic cylinder was placed in line with each cable. A servo valve controlled flow in and out of the cylinder. The control computer sensed cylinder position and cable tension force, and controlled the valve to achieve the force and position objectives.

Unfortunately, a given set of pre-tensions will not yield a unique positioning of the collar within the tunnel. The positions for pre-tensioning the cables were determined in the system set-up phase. The operator adjusted cylinder positions using a graphical user interface while monitoring collar position and orientation, as well as the tension.

### Multi-Cylinder Control Algorithm

Figure 6 shows the block diagram for the hydraulic control system. At the heart of the algorithm is the position controller, which controls the individual positions of the six cylinders. The controller for each of these six embedded loops had the form

$$i_{v,j} = -K_p(q_{j,d} - q_j) - K_d \dot{q}_j \quad (1)$$

where  $q_j$  is the position of the  $j^{\text{th}}$  cylinder,  $q_{j,d}$  is the corresponding desired position,  $i_{v,j}$  is the current to the servo valve, and  $K_p$ , and  $K_d$  are control gains.

The desired positions for the six cylinders were determined from three sources, corresponding to the three control functions. The mean position commands were determined from pre-tension and set-up positions controlled by the user via a graphical user interface. An additional position set representing yaw commands was superimposed on the mean positions. A third set of position commands determined by the damping control system could be added to the others. In the damping controller, a set of gains ( $K_{dx}$ ,  $K_{dy}$ ,  $K_{dz}$ ,  $K_{d\theta}$ ) determine the damping forces and moment from the measured motion rates. A mapping matrix assigns motions to the six cables to create these damping forces and moments. While some preliminary demonstration of the damping system was done with the assembled system, it was not used in the wind-on tests and will not be discussed further.

For the yaw control function, position commands were generated by the cylinder motion profiler. As Fig. 7 (a top view of the cable system) shows, the yaw angle  $\psi$  can be manipulated by changing the cable lengths  $\ell_i$ . The motion profiler algorithm uses the system geometry to compute the distances from the endpoints of the pitch axle (when yawed to the desired angle) to the cable pulleys. Subtracting these from the distances at zero yaw ( $\bar{\ell}_i$ ) yields the change in cable length, and hence the required displacement of the cylinder. Cable lengths were not measured explicitly, but once the correct nominal lengths were established in the experimental set-up, changes in the lengths could be measured from the hydraulic cylinder position sensors. This requires that we assume that elastic elongation in the cables is constant.

System control functions were implemented using a PC-type computer. The PC performs all user interface and fault reporting. Hydraulic control and other real-time activities are performed by a second processor embedded in the PC. The control processor was an 80486 contained on a DAP4200a Data Acquisition Processor from Microstar Laboratories. Communication between the host PC and the DAP takes place over the PCI bus. The DAP 4200a is equipped with 16 single-ended/8 differential analog input channels, which can be sampled at up to 769 kHz total throughput. The board has only two analog output channels so a pair of four-channel analog output expansion boards was added.

### **Learning Controller for YAW**

Yaw motion for the wire suspension was created by manipulating cable lengths with hydraulic actuators. The VFT system controller must learn each maneuver to produce the wind tunnel simulation as follows. The missile autopilot repeats a maneuver several times. The VFT control computer attempts to perform the yaw maneuver commanded by the autopilot. An acceptable initial maneuver, in the absence of better information, is  $\Psi = 0$  (no yaw). After each maneuver iteration, the VFT controller updates the yaw motion in response to balance feedback from the previous iteration, and performs the revised maneuver. By repeating this process, the learning controller converges on a motion that closely mimics the free-flight behavior of the missile. The “true” maneuver is the one in which there is no yawing moment transmitted to the collar (balance), for this is the situation where aerodynamic loads are matched by the angular accelerations. This is the yaw maneuver that the missile would undergo in free flight. The algorithm has several advantages, including that it prevents dynamic VFT/autopilot interactions.

Figure 8 shows the operation of the learning controller. At each iteration  $i$ , the learner uses the results of the previous maneuver to compute a yaw trajectory for the following test. Based on the desired yaw, the cylinder motion profiler calculates a set of cylinder position time histories, and embedded cylinder position loops operate the cylinder position servos during the subsequent test.

We have developed a learning algorithm and tested it in computer simulations.<sup>6</sup> The origins of the algorithm lie in a qualitative understanding of the behavior of the missile, described heuristically here.

We begin with the dynamic torque balance for the missile:

$$I_{zz}\ddot{\Psi} = N \quad (2)$$

where  $I_{zz}$  is the yaw inertia,  $\Psi$  is the yaw angle (with the double dots indicating its second time derivative), and  $N$  is the measured yawing moment. We could simply integrate the measured moment to determine the yaw angle, using the learning rule:

$$\begin{aligned}
\ddot{\Psi}_{i+1,n} &= N_{i,n} / I_{zz} && \text{(Acceleration)} \\
\dot{\Psi}_{i+1,n+1} &= \dot{\Psi}_{i+1,n} + \ddot{\Psi}_{i+1,n} \Delta T && \text{(Velocity)} \\
\overline{\Psi}_{i+1,n+1} &= \overline{\Psi}_{i+1,n} + \dot{\Psi}_{i+1,n} \Delta T + \frac{1}{2} \ddot{\Psi}_{i+1,n} \Delta T^2 && \text{(Yaw Change)} \\
\Psi_{i+1,n+1} &= \Psi_{i,n+1} + \overline{\Psi}_{i+1,n+1} && \text{(New Yaw Profile)} \\
\text{at } \{n \leq 0\}, \overline{\Psi}_{i+1,n} &= \dot{\Psi}_{i+1,n} = 0 && \text{(Initial Condition)}
\end{aligned} \tag{3}$$

Here, first index denotes the experiment iteration and the second index denotes the time step (of duration  $\Delta T$ ) within the discrete-time signals. The acceleration is computed from the moment, and is integrated to get the yaw rate. The velocity and acceleration are used to compute the change in yaw angle  $\overline{\Psi}_{i+1}$ , which is added to the yaw angle function from the previous iteration ( $i$ ) to obtain the yaw angle at the next ( $i+1$ ) time step. However, the onset of motion would change the moments. The yawing moments that will be applied to the missile result from active control via actuators, as well as the aeroelastic and aerodynamic stability properties. In general, we do not know what these are.

For a missile with positive static stability and damping, the motion would tend to decrease the moment and imposed velocity would decay. With the algorithm described above, the controller would attempt a continuous yaw acceleration because, absent this motion, a constant yaw movement might be observed. Thus, we devised the following yaw change algorithm:

$$\begin{aligned}
\ddot{\Psi}_{i+1,n} &= (N_{i,n} / I_{zz}) \cdot W_{i,n} && \text{(Acceleration)} \\
\dot{\Psi}_{i+1,n+1} &= \dot{\Psi}_{i+1,n} e^{-\Delta T / \tau_v} + \ddot{\Psi}_{i+1,n} \Delta T && \text{(Velocity)} \\
\overline{\Psi}_{i+1,n+1} &= \overline{\Psi}_{i+1,n} + \dot{\Psi}_{i+1,n} \Delta T + \frac{1}{2} \ddot{\Psi}_{i+1,n} \Delta T^2 && \text{(Yaw Change)} \\
\text{at } \{n \leq 0\}, \overline{\Psi}_{i+1,n} &= \dot{\Psi}_{i+1,n} = 0 && \text{(Initial Condition)}
\end{aligned} \tag{4}$$

Here,  $W_{i,n}$  is a weighting function, used to weight response to moment in favor of those that occur just after a change in moment. That is, it is based on the idea that when a control moment is applied, the missile will move to a new equilibrium condition where the moment is minimized until the applied moment changes. The weighting function is computed by first processing the first-backward-difference of the moment with a low-order filter:

$$\bar{W}_{i,n} = (N_{i,n} - N_{i,n-1}) \left( 1 - e^{-\frac{\Delta T}{\tau_w}} \right) + \bar{W}_{i,n} e^{-\frac{\Delta T}{\tau_w}}$$

$$\bar{W}_{i,n} = 0 \text{ for } \{n = 0, -1\}$$
(5)

and then normalizing it by its largest value:

$$W_{i,n} = |\bar{W}_{i,n}| / \max(\bar{W}_{i,n})$$
(6)

The filter is a low-pass in series with a differentiator, so that it passes changes in the moment but decays to zero output if the moment is constant. The decay time is characterized by the time constant  $\tau_w$ .

This learning law also incorporates an exponential velocity decay term, characterized by the time constant  $\tau_v$ . The combination of the weighting filter and the velocity filter is that under constant moment, the acceleration and velocity both decay to zero.

Note that the stated assumptions about missile stability are not always true, and we must add a term to accommodate this inaccuracy. The final step in the learning law in Eq. (4) above is:

$$\Psi_{i+1,n} = \Psi_{i,n} + \bar{\Psi}_{i+1,n} - K_m N_{i,n}$$
(7)

where the new term is proportional to the measured moment by the constant  $K_m$ .

### Test Facility

The tests were conducted in the HIVAS facility at the Naval Air Warfare Center, China Lake, CA. HIVAS is part of the Weapons Survivability Laboratory. The facility, shown in Fig. 9, produces a free jet with air ducted from the bypass fans of four TF33 P11 turbofan engines. As configured for this test, HIVAS can produce a 56 in. diameter jet at speeds up to 550 kts. HIVAS can be rotated to face a number of test pads. Air exhausts into the desert environment. The wire suspension system was attached to a steel frame that represented the structure around a wind tunnel test section.

### BOA Missile Model

The BOA-1SC PTV-2 model was chosen because it had been used in prior wire suspension tests at HIVAS and because parts were available for use in the test. It is an advanced variant of the AIM-9 Sidewinder. Figure 10 shows the model geometry. For these tests, the hot-gas servomotors in the missile were powered from a compressed-air bottle located at the aft end of the missile in the rocket motor casing. The weight of the bottle accounted for the missing propellant, allowing the CG to be located at a mid-burn position, coinciding with the location of the pitch axle. A slip ring at the back of the model provided signal and power transmission.

The missile autopilot was equipped with rate feedback, and absolute angle measures were not available. The effect of this on the test results will be seen later. When, for example, the missile is programmed for steady level flight, the controller was attempting to hold a zero pitch rate. When the missile is disturbed from a pitch angle  $\Psi = 0$ , the controller will stop the pitch motion (restore  $\dot{\Psi}$  to zero) but will not return the missile to  $\Psi = 0$ . In fact, the autopilot will fight a return to a level orientation because this would involve a non-zero pitch rate. The control in the pitch and yaw planes are identical, except when a maneuver is commanded in one of them.

One hope for these tests was to reproduce the roll-locking observed in flight tests. Roll-lock is a behavior wherein the missile, which rolls freely at low angles of attack, stops rolling suddenly when the angle of attack increases. Demonstration of roll-lock was important because it would show that key missile stability characteristics could be recreated in VFT.

## **Wind-On Tests**

### *Data Acquisition*

Data was acquired by two methods during the tests. All signals available to the VFT computer were recorded at 416 Hz (2400  $\mu$ s intervals). Other signals were recorded by the missile telemetry system. These signals were logged at 1390 Hz (720  $\mu$ s intervals).

### *Test Procedure*

Each test began with the missile in a zero-pitch condition. A ring on the end of a rod was placed over the missile nose. A person standing ahead of the test frame and below the air stream held the rod.

The facility operator brought the airflow velocity to the desired condition. The missile operator powered up the missile, activated the air supply, switched the missile to operation from internal power, and then disconnected

external power. The autopilot was initiated by removing the external power. The missile operator would then give the command to remove the nose ring. The ring was pulled away from the missile, and the test flight began.

The test team completed seven virtual flights during the first test window at HIVAS. The tests are summarized below. Figures 10 through 18 contain several of the recorded variables for the tests.

The intent of the test sequence was to demonstrate proof-of-concept. While the balance was calibrated in a single-axis load apparatus, we did not apply test loads on the installed balance or otherwise attempt to assess the load measurement accuracy. Thus, we make no statements about load measurement accuracy. The qualitative trends in the data do demonstrate the system function.

## **Results and Discussion**

### *Test 2 (Fig. 11)*

Flight Control Program: Pitch rate = 0

Velocity: 350 kts

The missile held zero angle of attack for about 8 seconds. It rolled rapidly for about 1.5 second. There was then a pitch up to about 5 deg. The missile roll-locked in this position and approximately held its attitude until the autopilot program ended. Roll-locking consists of zero or near zero roll rates. We observed mild cable vibration and some body bending, but all systems functioned properly.

Balance and inertial sensors onboard the model show an oscillation in yaw at about 9 Hz. This probably involves missile aeroelastic characteristics coupled with the elasticity of the mount.

### *Test 3 (Fig. 12)*

Program: Pitch rate = 0

Velocity: 400 kts

The behavior was similar to that in Test 2. The autopilot was able to hold the pitch rate at zero for long periods. After a pitch up to about 5 deg, the missile again roll-locked. There is still some occasional rolling, wherein the BOA would roll about 30 deg suddenly, and then stop or roll very slowly. This test demonstrated that we could test at 400 kts.

### *Test 6 (Figs. 13, 14)*

Program: Pitch cycle (S-turn)

Velocity: 350 kts

The pitch rate command for this flight can be seen in Fig. 13. The missile can be seen to execute the maneuver in Fig 14. While we do not have flight data against which to quantitatively benchmark the result, it shows that the constrained model can execute a programmed maneuver.

All three of the tests just discussed show both yaw excursions and yawing moments, although the yaw motion feature was not activated. The excursions are a result of compliance in the cable systems. The yawing moment results as the autopilot attempts to prevent additional yaw motion (i.e., non-zero yaw rate).

#### *Learning Controller Tests*

Experiments to demonstrate the operation of the learning controller and the upgraded balance took place in the HIVAS facility using the BOA missile described earlier, but approximately 9 months after the initial tests. Between the test sequences, the balance was modified for greater sensitivity in the lateral plane. The experimental series consisted of eight virtual flights.

Tests 10 through 15, again conducted at 350 kts, were the runs in which iterative learning was attempted. The missile controller was commanded to perform the horizontal-plane s-maneuver. In Run 10, the yaw was held at 0 deg. It was updated in subsequent runs based on the measured yaw restraining moment until the yaw moment was small.

Time permitted only a single training sequence, but the initial sequence was sufficient to demonstrate the function of the learning algorithm.

Figure 15 shows the results of the learning iterations. The learning law parameters are shown in Table 1. For each run, the plots show the measured moment and the yaw attempted by the VFT controller for each case. In Run 10, the moment is slightly saturated. It was nevertheless useful for updating the yaw command.

In the first attempt at learning, the algorithm overcorrected the yaw, resulting in the badly- saturated moment measured in Run 11. This is corrected in the subsequent run by reducing the balance gains and increasing the calibration parameters. Run 13 shows only minor changes in the yaw.

Figure 16 compares the moment measured in Runs 10 and 15. The controller has substantially reduced the measured moment by identifying the appropriate yaw time history. This plot is the showpiece from this test sequence in that it captures the ability of the algorithm to iteratively reduce the measured yaw.

Figure 17 compares the side force measured in Runs 10 and 15. The side force measurements have been filtered in post-processing. This demonstrates the ability of the improved balance to measure side forces. In Run 10, the side force was small. In Run 15, it is much larger because the missile is executing the s-maneuver in the yaw plane.

We conclude from the reduction in yawing moment with each increasing iteration that the controller is learning the maneuver. We lack a solid benchmark in the pitch plane against which to compare the result, but the similarity in trends corroborates the yawing moment data. The only significant deficiency of the demonstration is that the algorithm was unable to correct the initial peak in the yaw moment within the number of iterations available.

### **Conclusions**

The test technique described here provides a means of testing missile guidance and control systems in the wind tunnel. Test experience has shown safe operation of the system using an Air-to-Air missile, demonstrating that dynamic characteristics such as roll locking, which appeared in flight tests, can be recreated in the wind tunnel. The tests showcased a new balance with pitch and roll freedom. Hydraulic control provides yaw and cable tension control, with the option to damp structural oscillations using accelerometer feedback. The latter has not yet been demonstrated. The sequence of virtual test flights demonstrated a repetitive-learning controller that uses balance feedback to simulate yaw maneuvers. Much of the system – the hydraulic modules, cable assemblies, and pitch-roll collar, could be put into service in wind tunnel tests. The measurement techniques and the learning controller have been demonstrated at a basic level, but more test experience is required to refine these methods.

Future work should include testing with a model that can sustain longer runs, refinement of dumping control for the cables, and tests in which forces or flows are compared to those for sting-mounted models to quantify aerodynamic interference.

## References

1. Ratliff, C. L. and Marquart, E. J., "An Assessment of a Potential Flight Test Technique: Virtual Flight Testing, @ AIAA 95-3472, AIAA Atmospheric Flight Mechanics Conference, August 7-9, 1995.
2. Lawrence, C. and Mills, B., "Status Update of the AEDC Virtual Flight Testing Development Program", AIAA 2002-0168, 40th Aerospace Sciences Meeting and Exhibit, January 14-17, 2002, Reno, NV.
3. Magill, J. C. and Wehe, S. D., "Initial Test of a Wire Suspension Mount for Missile Virtual Flight Testing," AIAA Paper 2002-0169, 40th AIAA Aerospace Sciences Meeting and Exhibit, 14-17 January 2002, Reno, NV.
4. SKF Catalog, Cat. 4000 US, 1991.
5. Brandlein, Johannes, Eschmann, Paul, Hasbargen, Ludwig, Weigand, Karl, Ball and Roller Bearings: Theory, Design, and Application, 1999, John Wiley and Sons, Chichester.
6. "Active Yaw Control with a Wire Suspension System for Dynamic Wind Tunnel Testing." Magill, J.C., Cataldi, P., Morency, J.R., and Hammer, D.X., Burgess, R., and Jeter, E., AIAA Paper No. 2005-1295, 43rd AIAA Aerospace Sciences Meeting and Exhibit, 10-13 Jan 2005 - Reno, Nevada, November 2004.
7. Brandlein, Johannes, Eschmann, Paul, Hasbargen, Ludwig, Weigand, Karl, Ball and Roller Bearings: Theory, Design, and Application, 1999, John Wiley and Sons, Chichester.
8. Graewe, Eberhard, Ewald, Bernd, and Eckert, "Design and construction of internal balances for the German/Netherlands Wind Tunnel (DNW)," First International Symposium on Internal Strain Gauge Balances, NASA Langley Research Center, March 1999.
9. Rhew, Ray D., "NASA LaRC Strain Gage Balance Design Concepts," First International Symposium on Internal Strain Gauge Balances, NASA Langley Research Center, March 1999.
10. Mole, P.J., "Development of a Six-Component Flexured Two-Shell Internal Strain Gage Balance," AIAA 93-0793, 31st Aerospace Sciences Meeting, Reno, NV, January 11-14, 1993.
11. Crandall, Stephen H., Dahl, Norman C., and Lardner, Thomas J., An Introduction to the Mechanics of Solids, Second Edition, McGraw-Hill, New York, 1978.

## Acknowledgement of Support and Disclaimer

This material is based on work supported by the US Air Force Arnold Engineering Development Center under Contract No. F40600-01-C-0015. The contract monitor is Mr. Ronald Bishel. The authors thank Frank Steinle, Clark Lawrence, and Ben Mills of Sverdrup/AEDC for their helpful input.

Any opinions, findings and conclusions or recommendations expressed in this material are those of the author(s) and do not necessarily reflect the views of the US Air Force Arnold Engineering Development Center.

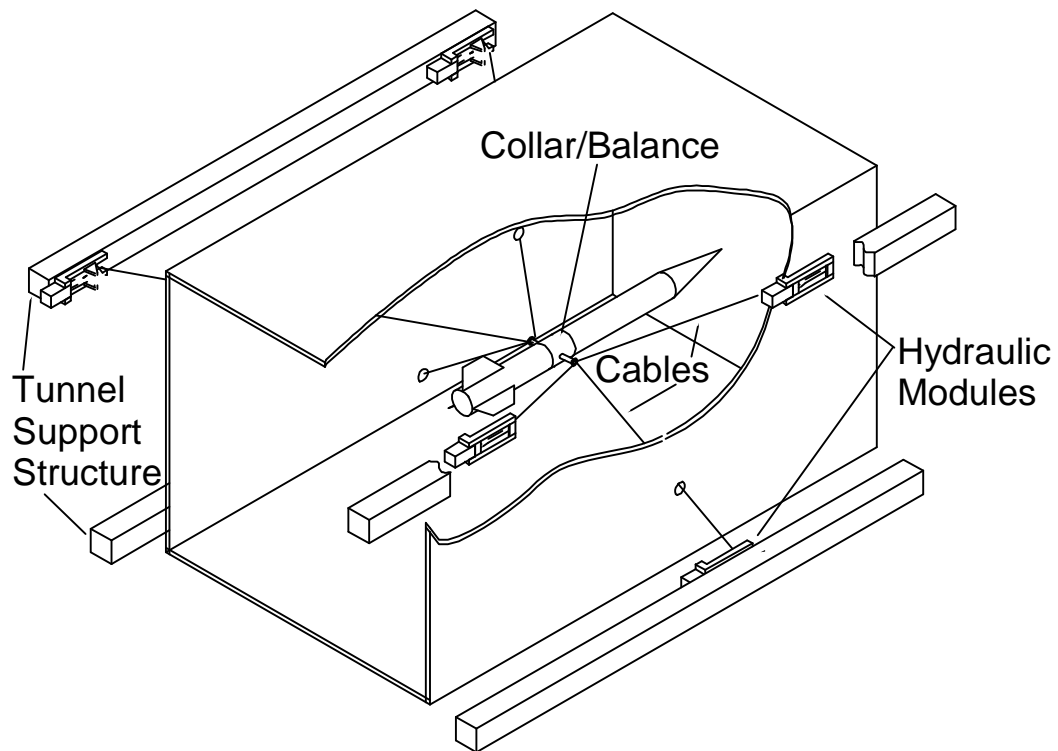


**Fig. 1 Configuration of wire suspension system, shown in representative wind tunnel test section**

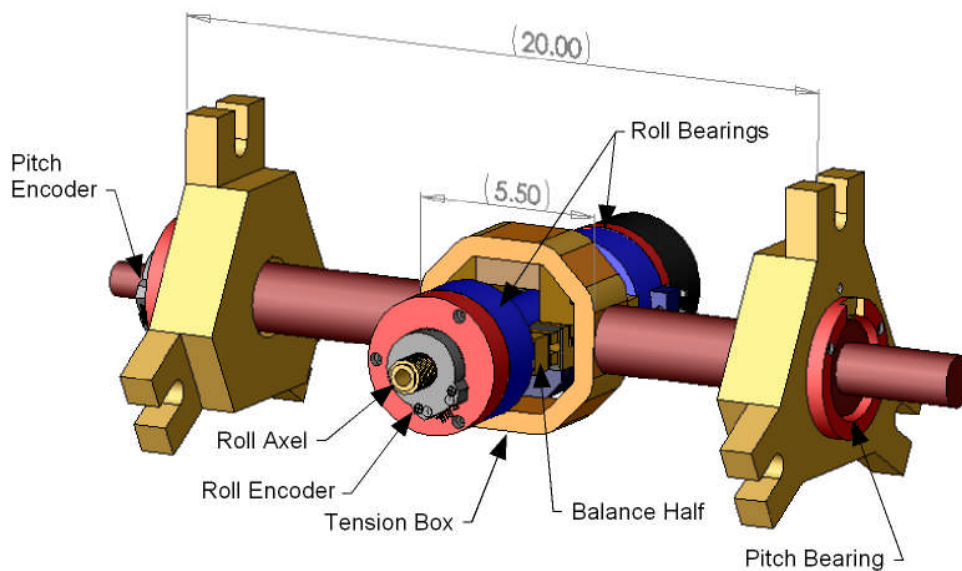


**Fig. 2 Collar assembly supports missile fore and aft sections and provides free pitch and roll. The balance segments were instrumented to provide force and moment measurement**

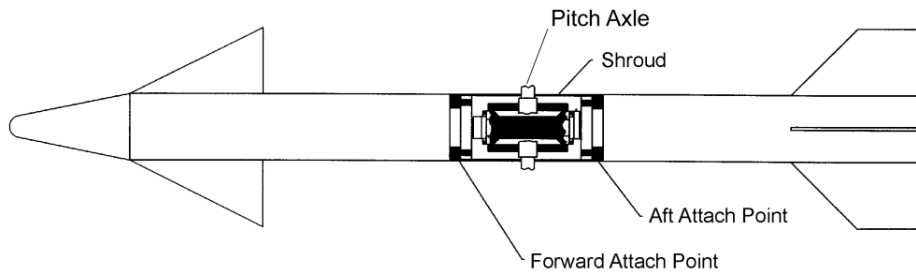


**Fig. 3 Missile attachment to collar assembly**

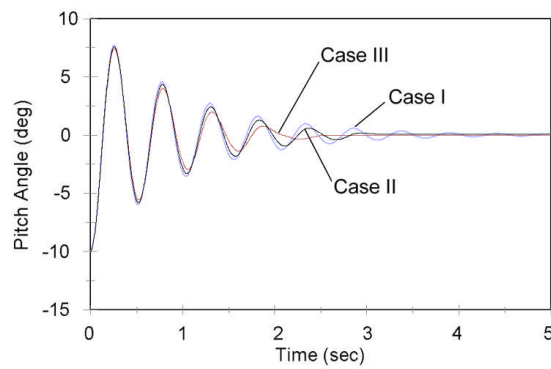


**Fig. 4 Simulated pitch response of a model disturbed 10 deg. from its trim angle-of-attack for three different bearing friction levels. Case I: No rolling or starting friction, Case II: 12 in.-lb rolling torque/24 in.-lb starting torque, and Case III: 30 in.-lb rolling torque/60 in.-lb starting torque**

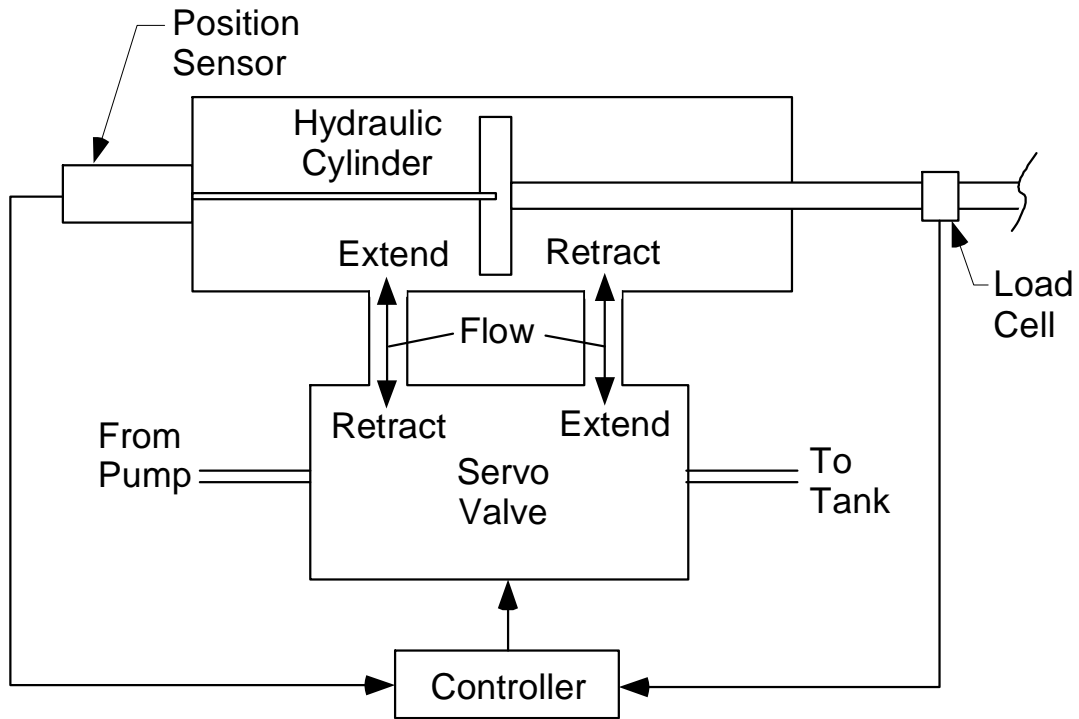


Fig. 5 Components of hydraulic control system

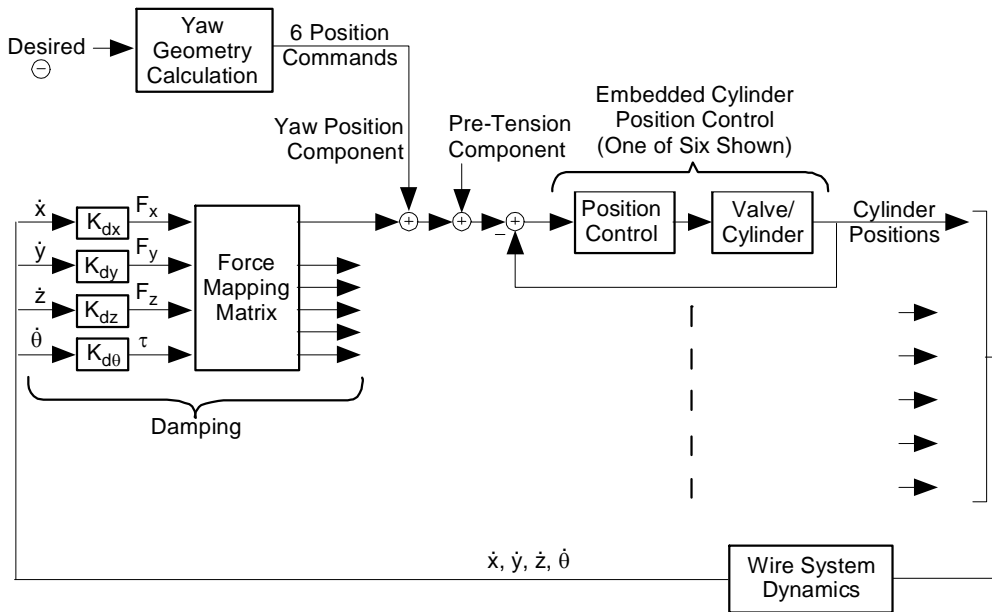
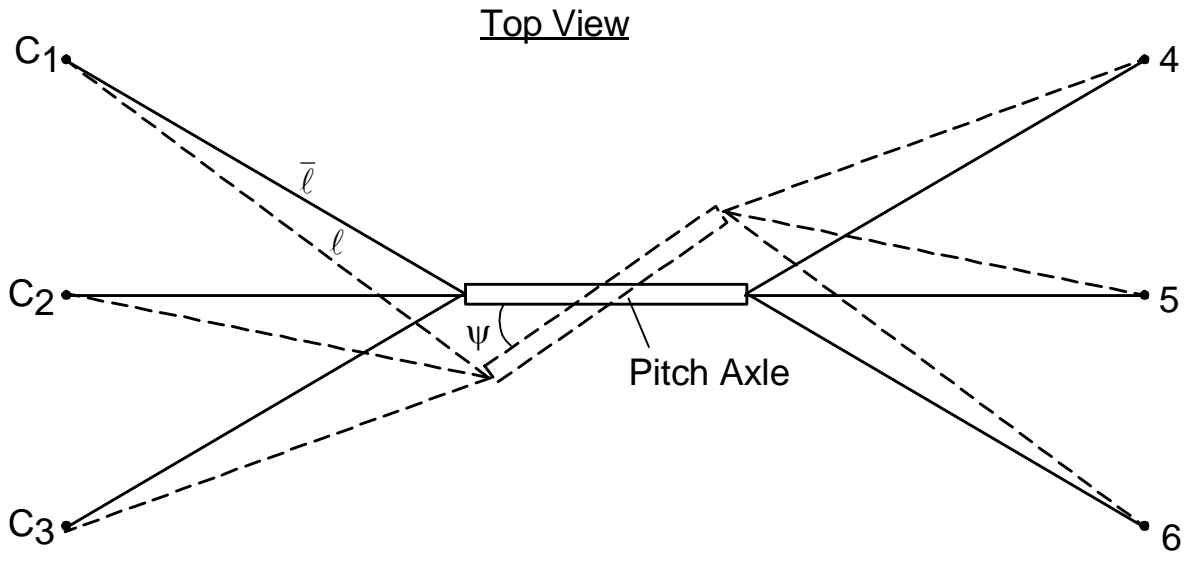
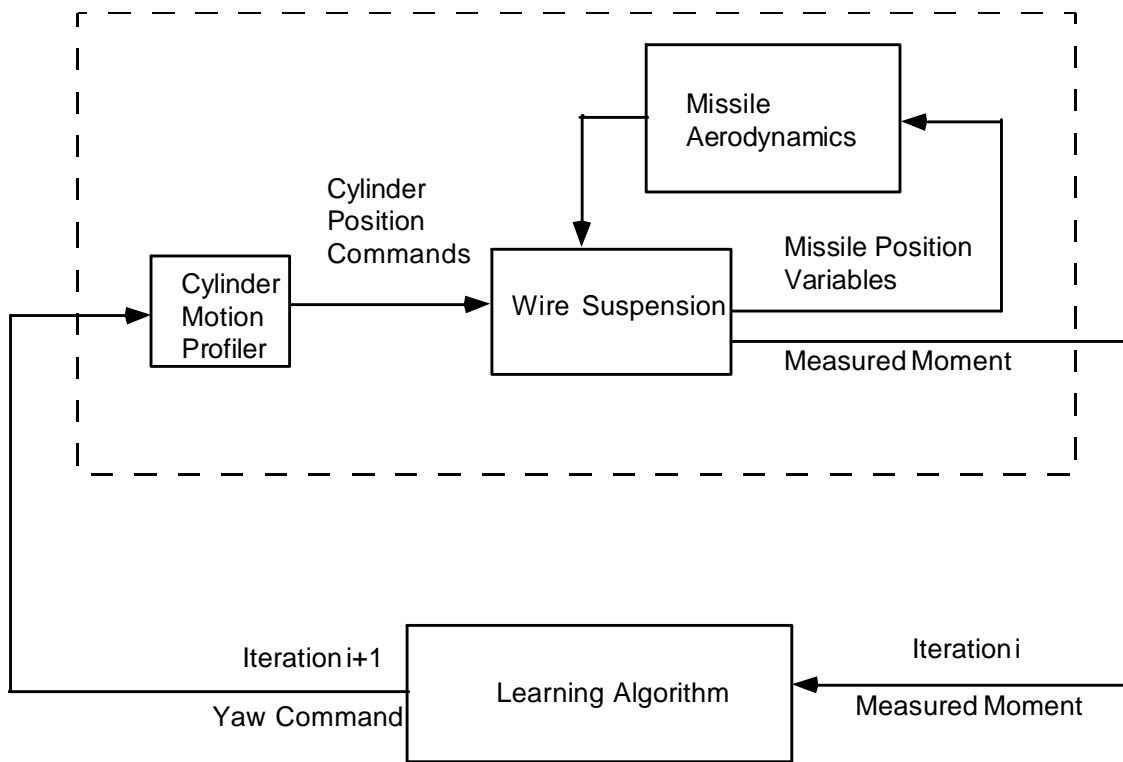


Fig. 6 Block diagram of hydraulic control signal flow



**Fig. 7** Top view of cable geometry shows how cable lengths are related to yaw position



**Fig. 8** Learning Controller Signal flow

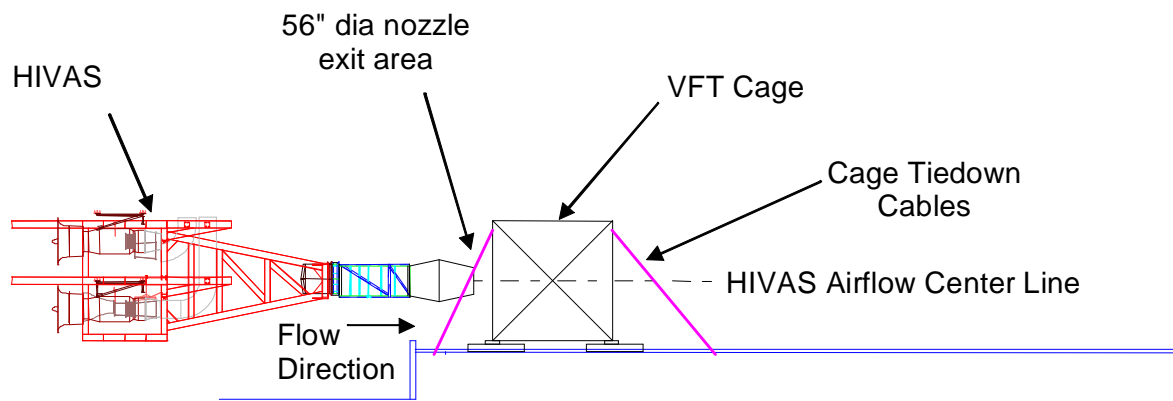


**Fig. 9 HIVAS Facility at Naval Air Warfare Center, China Lake, CA**

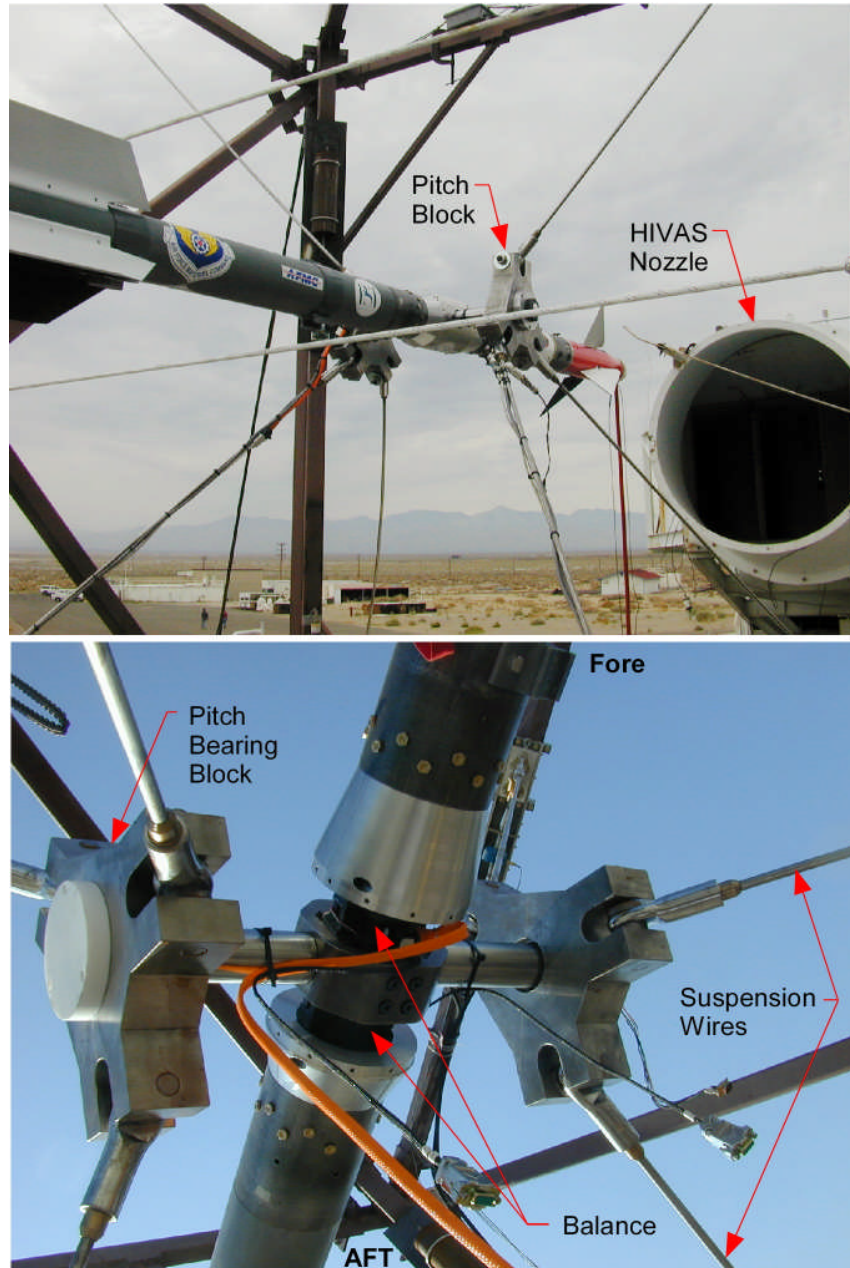


**Fig. 10 BOA Missile Model Attached to VFT Collar**

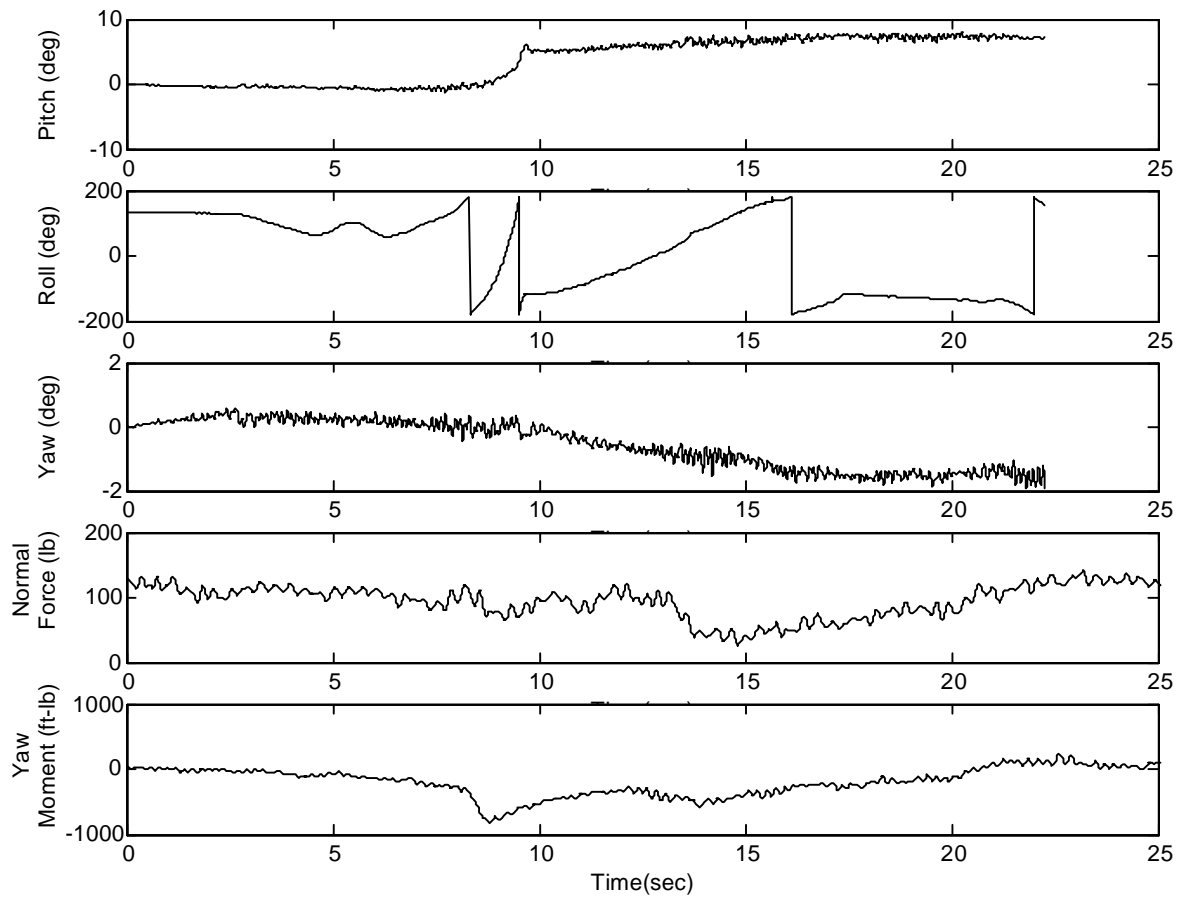


**Fig. 11** Motion and force measurements on the model during Test 2: 350Kt flow velocity with autopilot programmed for zero pitch rate

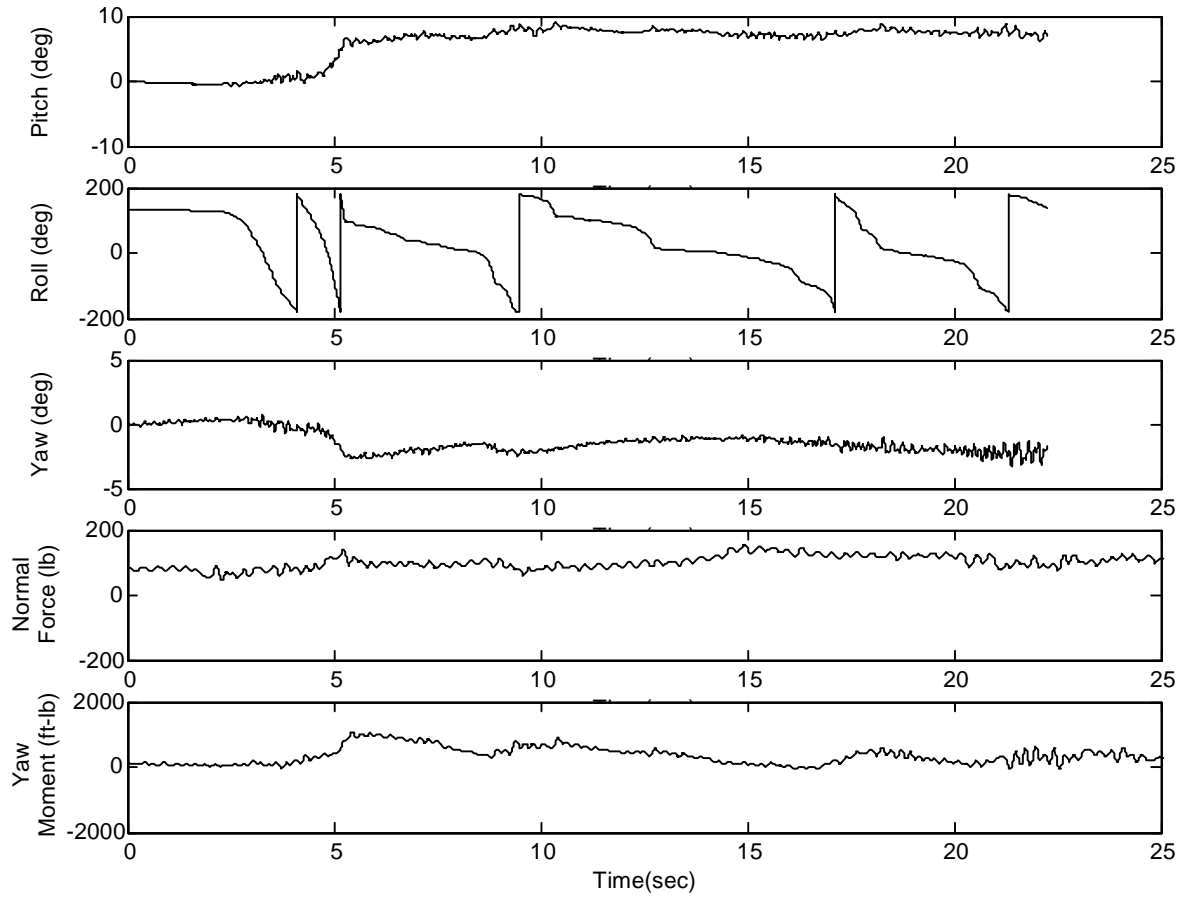


**Fig. 12 Motion and force measurements on the model during Test 3: 400Kt flow velocity with autopilot programmed for zero pitch rate**

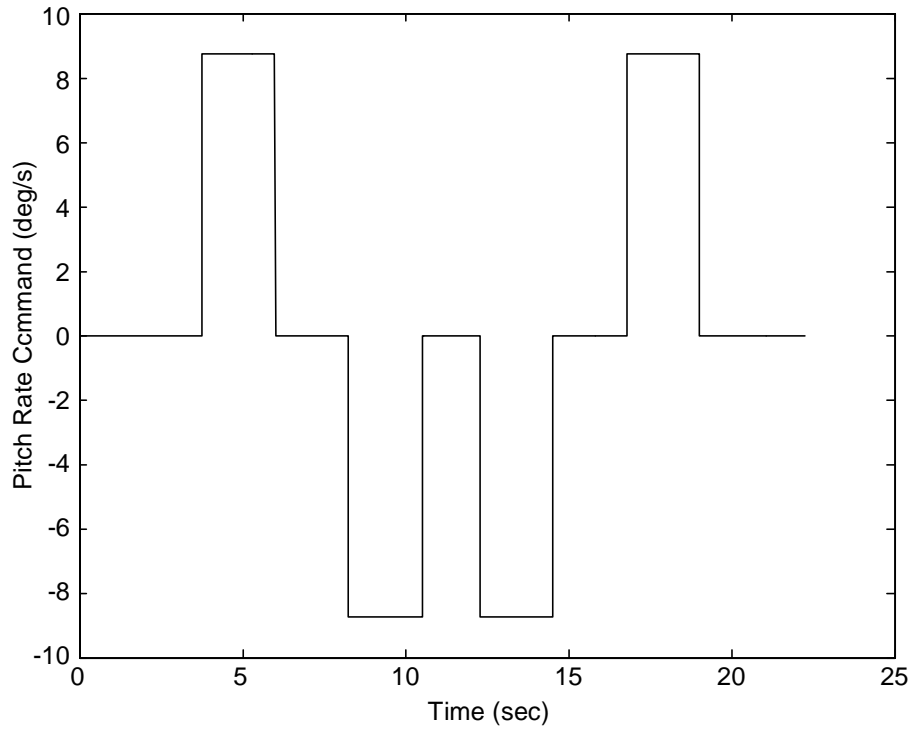


**Fig. 13 Pitch motion command for Test 6 (see Fig. 14)**

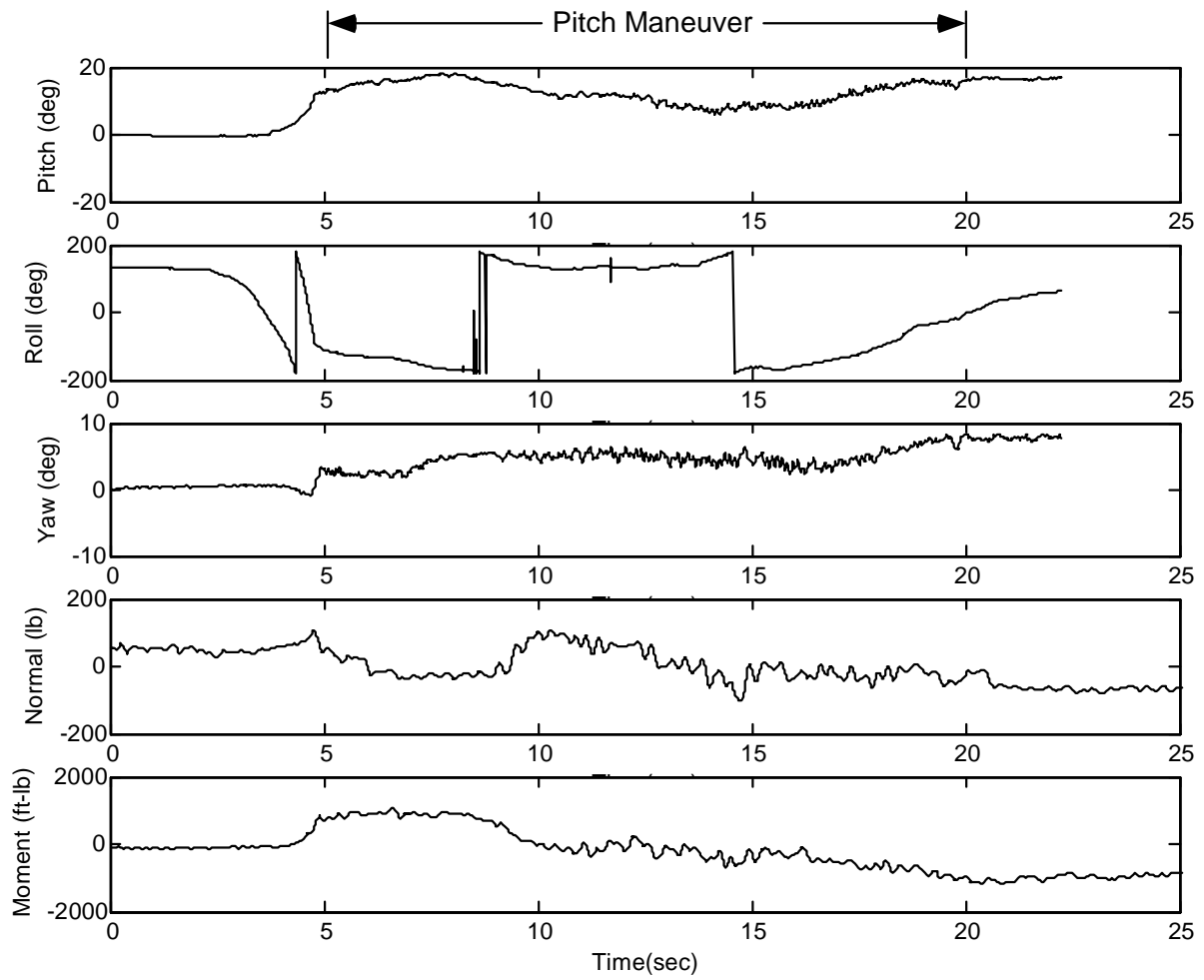


**Fig. 14** Motion and force measurements on the model during Test 6: 350Kt flow velocity with an s-turn maneuver in the pitch plane

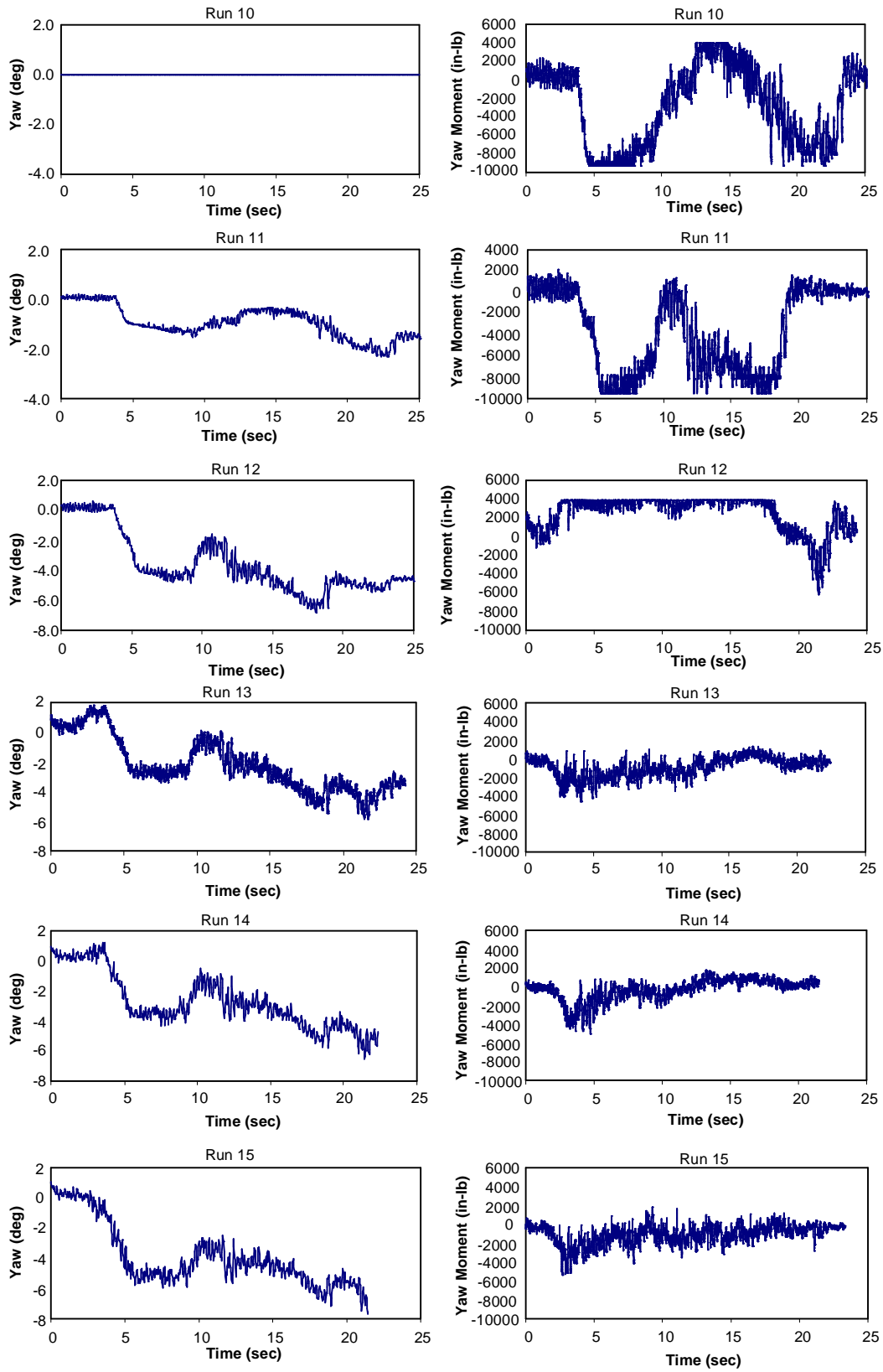
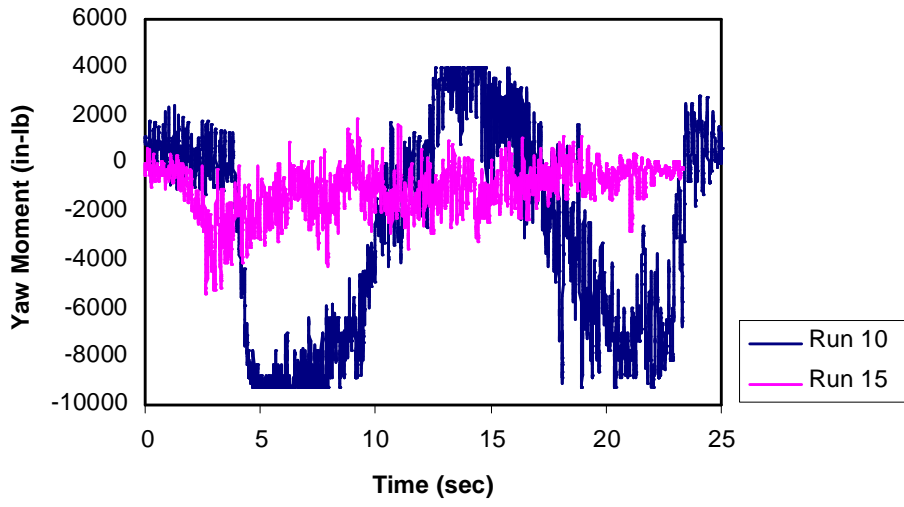
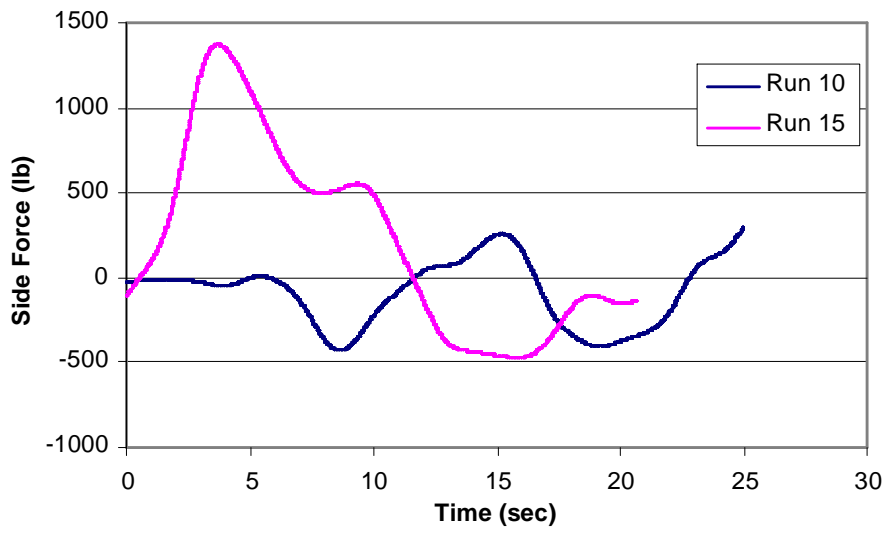


Fig. 15 Comparison of commanded yaw and measured moment for six learning iterations



**Fig. 16** Comparison of measured moment for the first (Run 10) and last (Run 15) learning iterations



**Fig. 17** Comparison of (filtered) side force in Runs 10 and 15

**Table 1 Learning law parameters**

<b>Run</b>	<b>I (slg-ft<sup>2</sup>)</b>	<b><math>\tau_v</math> (s)</b>	<b><math>\tau_w</math> (s)</b>	<b>K (deg-m/N)</b>
10	500	0.01	0.005	-0.0002
11	500	0.01	0.005	-0.0003
12	500	0.01	0.005	-0.0003
13	500	0.01	0.005	-0.0003
14	500	0.01	0.01	-0.0003